Research Article

Dual color localization microscopy of cellular nanostructures

Manuel Gunkel[1], Fabian Erdel[2], Karsten Rippe[2], Paul Lemmer[1], Rainer Kaufmann[1], Christoph Hörmann[1], Roman Amberger[1] and Christoph Cremer[1,3,4]

[1] Kirchhoff-Institute for Physics & BioQuant Center University of Heidelberg, Heidelberg, Germany
[2] Deutsches Krebsforschungszentrum & BioQuant Center University of Heidelberg, Research Group Genome Organization & Function, Heidelberg, Germany
[3] Institute for Pharmacy and Molecular Biotechnology, University of Heidelberg, Heidelberg, Germany
[4] Institute for Molecular Biophysics, The Jackson Laboratory, Bar Harbor, ME, USA

The dual color localization microscopy (2CLM) presented here is based on the principles of spectral precision distance microscopy (SPDM) with conventional autofluorescent proteins under special physical conditions. This technique allows us to measure the spatial distribution of single fluorescently labeled molecules in entire cells with an effective optical resolution comparable to macromolecular dimensions. Here, we describe the application of the 2CLM approach to the simultaneous nanoimaging of cellular structures using two fluorochrome types distinguished by different fluorescence emission wavelengths. The capabilities of 2CLM for studying the spatial organization of the genome in the mammalian cell nucleus are demonstrated for the relative distributions of two chromosomal proteins labeled with autofluorescent GFP and mRFP1 domains. The 2CLM images revealed quantitative information on their spatial relationships down to length-scales of 30 nm.

Received 9 January 2009
Revised 10 May 2009
Accepted 14 May 2009

Supporting information available online

Keywords: Chromatin · 2CLM · Localization microscopy · Molecular imaging · Nanobiophotonics · SPDM · Spectrally assigned localization microscopy (SALM) · Superresolution fluorescence microscopy

1 Introduction

About 170 years ago, light microscopy facilitated the discovery of the cell as the fundamental unit of life, thus initiating one of the great revolutions of human science (for review see ref. [1]). In the development of modern cell biology and its biomedical applications, however, analysis methods using visible light microscopy approaches often played a secondary role compared with biochemical techniques. A major reason for this was the optical resolution thought to be restricted to a fundamental limit of a few hundreds of nanometers laterally (and about 600 nm axially). Consequently, the nanostructure of cellular machines (*e.g.* the protein complexes responsible for molecular transport, DNA replication, transcription and repair, RNA splicing, protein synthesis, and degradation), was not accessible to light microscopy. The same is true for the spatial organization of specific chromatin domains with a size in the hundred nanometer range that play an essential role for gene regulation [2]. As described in the famous publication of Ernst Abbe (1873) [3], this limit in light-optical resolution of about 200 nm was thought to be due to the wave nature of light; it was regarded to be insurmountable according to the fundamental laws of physics. A very similar conclusion was obtained in 1896 by Lord Rayleigh [4]. However, a variety of laseroptical far field microscopy techniques based on fluorescence excitation has been developed recently to circumvent the Abbe/Rayleigh-limit of 200 nm. These make the light-optical analysis of biological

Correspondence: Professor Christoph Cremer, Institute for Molecular Biophysics, The Jackson Laboratory, 600 Main Street, Bar Harbor, ME 04609, USA
E-mail: cremer@kip.uni-heidelberg.de.
Fax: +49-6221-54-9271

Abbreviations: 2CLM, two color localization microscopy; **PALM,** photoactivated localization microscopy; **ROI,** region of interest; **SALM,** spectrally assigned localization microscopy; **SPDM,** spectral precision distance microscopy

macromolecules with enhanced resolution possible. Some well-known methods are 4Pi-Microscopy [5, 6], structured/patterned illumination microscopy [7, 8], STED microscopy [9, 10], and spectrally assigned localization microscopy (SALM) approaches using far field fluorescence microscopy (P. Lemmer, C. Cremer, D. Baddeley, H. Eipel, submitted application for patent on March 19, 2008; C. Cremer, *et al*. German Patent Application No. 196.54.824.1/DE, submitted Dec 23, 1996) [11–28, 29–32]. With these techniques, an effective optical resolution in the 10–20 nm regime has been obtained. While STED microscopy is a focused beam method that allows it to rapidly image small regions of interest (ROIs, few micrometer extension), the complementary localization microscopy techniques are preferentially used in a nonfocusing setup for rapidly imaging large ROIs (50–100 μm extension).

The basis of SALM as a far field fluorescence microscopy approach is the independent localization of "point-like" objects excited to fluorescence emission by either focused or nonfocused illumination techniques, typically with a laser. This means the localization is achieved by appropriate features of the fluorochromes resulting in an "optical isolation". We refer to this approach as "spectral precision distance (position determination) microscopy" (SPDM). SPDM was already conceived and realized in proof-of-principle experiments in the 1990s [11–16, 19]. Compared with related concepts [33–35], the SPDM approach relies on specific spectral signatures including all kinds of fluorescence emission parameters suitable, from absorption/emission spectra to fluorescence life times [13] to luminescence properties in general.

In the last few years, SALM methods have been improved considerably by several groups by making use of photoswitchable fluorochromes. In these approaches, fluorochromes are switched between a "dark" state A and a "bright" state B using a first laser wavelength λ_1 for switching from A to B and a second laser wavelength λ_2 from B to A. In this way, the position of the molecules was determined with precision values significantly better than the full width at half maximum (FWHM). These microscopic techniques were termed photoactivated localization microscopy (PALM) [20], fluorescence photoactivation localization microscopy (FPALM) [21], stochastic optical reconstruction microscopy (STORM) [22], PALM with independently running acquisition (PALMIRA) [23, 24], or "direct" STORM (dSTORM) [27]. In all these approaches, special fluorochromes were used that can be photoswitched between a "dark" state A and a "bright" state B [6].

Recently, we applied SPDM on the nanometer resolution scale to conventional fluorochromes. In contrast to the photoswitching-based SALM methods cited above, only one laser wavelength is used to induce fluorescence/luminescence lifetimes in a given fluorochrome on the second time scale. In this case "reversible photobleaching" [25, 26, 28] occurs. "Reversible photobleaching" has been shown to be a general behavior of several fluorescent proteins, *e.g*. GFP derivates like CFP, GFP, citrine, or eYFP [36–38]. Under such conditions, the fluorescence emission of certain flurophores can be described by assuming three different states of the molecule: A fluorescent state M_{fl}, a long-lived reversibly bleached state M_{rbl}, and an irreversibly bleached state M_{ibl}. Once the molecule returns from the M_{rbl} state to the M_{fl} state, it can be excited a large number of times (fluorescence bursts) until it passes into the irreversibly bleached state M_{ibl} (*i.e*. a dark state of a lifetime which is long compared with the acquisition time [36, 39]).

Thus, its position can be determined with nanometer precision [25, 26, 28]. With transition time constants k_1, k_2, k_3, one can assume the transition scheme [36]:

$$M_{rbl} \underset{k_1}{\overset{k_2}{\rightleftarrows}} M_{fl} \overset{k_3}{\rightarrow} M_{ibl}$$

We recently showed that reversible photobleaching can be used for super-resolution imaging of cellular nanostructures labeled with conventional fluorochromes such as Alexa 488 [25, 39] or the green fluorescent protein variant YFP [26]. This novel extension of the SPDM approach to ordinary fluorophores was based on the possibility to produce the optical isolation required by allowing only one molecule in a given observation volume and in a given time interval to be in the M_{fl} state. Such conditions were achieved by using an excitation intensity in the 10 kW/cm^2 to 1 MW/cm^2 range. These conditions were equivalent to switching the majority of the fluorophores to a metastable dark state and allowing the spontaneous return to lower energy levels under the emission of fluorescence photons [29]. Recently, Fölling *et al*. [29] have described a related approach to obtain highly resolved dual-color images of immunostained microtubules and peroxysomes using Atto 532 and 565 dyes. Here we present first results to extend the SPDM method to the localization of two different molecule types in human cell nuclei [Two color localization microscopy (2CLM)]. Two types of nuclear proteins tagged with two different standard fluorescent proteins were distinguished by different fluorescence emission wavelengths. 2CLM was

applied to "nanoimage" the spatial distribution of these proteins at molecular optical resolution.

The organization of the DNA genome by proteins is a particular interesting subject for 2CLM microscopy studies. In the cell nucleus the DNA is compacted by histone proteins into a nucleoprotein complex termed chromatin [40]. The central building block of chromatin is the cylindrically shaped nucleosome (11 nm diameter, 5.5 nm height). It comprises an octamer core of two copies each of histones H2A, H2B, H3, and H4, around which the DNA is wrapped in 1.67 turns. In the present study the technique of 2CLM microscopy was used to determine the intracellular localization of chromatin remodeling complexes with respect to chromatin. Chromatin remodelers are molecular machines that can translocate nucleosomes along the DNA double helix upon hydrolysis of ATP [41–44]. By making use of autofluorescent constructs of histone H2A as a nucleosome/chromatin marker and the ATPase subunit Snf2H [43–45] that defines a certain class of chromatin remodeling complexes, their nuclear localization was analyzed with an estimated mean accuracy in the range of about 20 nm (*ca*. 1/25 of the excitation wavelength). The results reveal details on the interaction of remodeling complexes with chromatin at unprecedented effective resolution.

2 Materials and methods

2.1 Specimen preparation

Human U2OS osteosarcoma cells were cultured on 12 mm diameter glass coverslips in DMEM supplemented with 10% FCS for 1 day after plating. Cells were transiently transfected with plasmid vectors for Snf2H-GFP and H2A-mRFP1 using Effectene (Qiagen) according to standard protocols. After transfection, cells were cultured for 1 day, fixed in 4% paraformaldehyde, and then embedded with Mowiol 4–88 (Roth) as mounting medium. The plasmid pEGFP-N3-Snf2H was kindly provided by Patrick Varga-Weisz and contains the full coding sequence of human Snf2H fused to GFP at the C-terminus [45]. The plasmid pRSET-H2A-mRFP1 contains the full coding sequence of human H2A

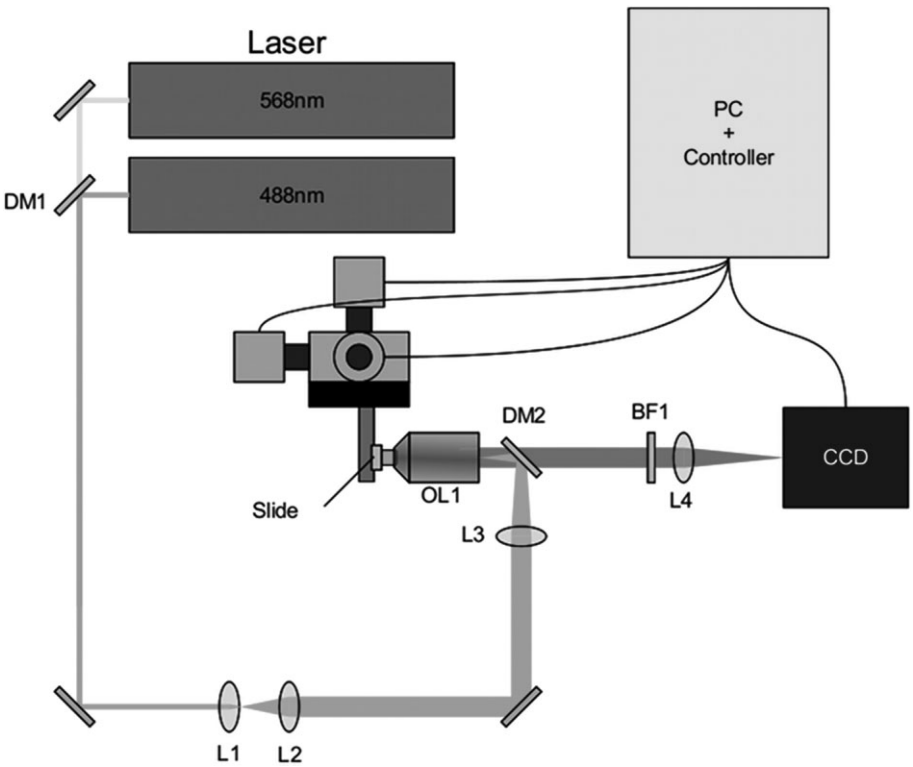

Figure 1. Microscope setup. Schematic representation of the microscopic setup for 2CLM. DM1, DM2: dichroic elements, L1–L4: lenses or lens systems, BF1 (interchangeable blocking filter): dichroic elements to block the illumination light (488 nm, 568 nm). GFP fluorescence emission (emission maximum @ λ_{em} = 520 nm) is transmitted through a bandpass filter (HQ 525/50), mRFP1 fluorescence emission (emission maximum @ λ_{em} = 584 nm) is transmitted through a triple line blocking filter (488/568/647 nm). From Lemmer *et al*. 2009 [47].

with the red fluorescent mRFP1 domain at the C-terminus [46].

2.2 Microscope setup

In Fig. 1 the principal microscope setup is shown schematically. Due to the "bright" initial state (M_{fl}) of the fluorochromes, specimens can be imaged in a standard far field conventional epifluorescence mode as well as in the 2CLM mode. The specimens were illuminated by an Ar^+-laser at λ_{exc} = 488 nm (excitation of GFP) or a Kr^+-laser at λ_{exc} = 568 nm (excitation of mRFP1), which were focused by the lens system L1–L3 and an objective lens 100×/NA1.4, oil (Leica, 35578 Wetzlar, Germany). This focusing was modified in such a way that fluorescent molecules in the observation volume were exposed to illumination intensities in the order of 50–200 kW/cm^2 within a large ROI. The degree of focusing and thus the laser power density was adjusted by varying the distances within the lens system along the optical axis. Under these conditions, suitable fluorochromes as GFP and mRFP1 exhibited their characteristic reversible photobleaching or light induced blinking, which was used to identify and spatially assign the localization of individual molecules. Up to 70 000 single molecules were detected in a ROI of about 20×20 µm^2. Using a sensitive CCD camera (PCO, 93309 Kehlheim, Germany) with a quadratic pixel size of 6.45×6.45 µm^2 (1376 × 1040 pixels total) with a quantum efficiency of up to 65% for image acquisition, time series of 2D-images were acquired with a repetition rate between 10–16 Hz. A typical time stack of 1 500 images was acquired within approximately 2 min. For further details, see ref. [28].

An estimation of the chromatic shift was obtained by imaging fluorescently labeled 100 nm beads under the same conditions used for the acquisition of 2CLM images. The positions were determined in both channels and compared to each other. The mean chromatic shift was found to be 5.6 ± 2.3 nm (see Supporting Information).

2.3 Software for data registration and evaluation

The recorded microscopy data were stored on a computer hard disk and evaluated later by algorithms implemented in MATLAB (7.0.1, The MathWorks, Natick, USA), a matrix based programming language for numerical computations. The algorithms were designed to handle the data with high background noise and large variation of background due to bleaching of the fluorochromes (*e.g.* dense labeling, large observation/activation volume) as well as for a low noise scenario with negligible bleaching (*e.g.* photoactivatable molecules in PALM/FPALM and/or small excitation volumes). The algorithm calculates the following quantities [26, 28]:

(i) The position of the fluorescence signal in the object plane/in the object space.
(ii) Estimates for the localization accuracy (parameter errors are the diagonal elements of the covariance matrix at convergence) on the single molecule level.
(iii) The characteristic parameters of the model function used to determine single molecule positions.
(iv) Estimates for the number of detected photons *per* molecule as a decisive parameter of localization microscopy.
(v) The position of the detected signal (individual molecule) in the data stack (*i.e.* image frame number) to analyze the influence of time and to extract relevant characteristics of the fluorochromes used.

Following signal detection and registration, in a second step an optional preprocessing was performed. While signals with high S/N (low background) can be used as raw data for the following data segmentation, in case of high background and photobleaching effects, an additional computing step was performed to segment signals originating from single molecules only. For this a differential photon stack $D_{Ph}(x, y, t') = S_{Ph}(x, y, t_{k+1}) - S_{Ph}(x, y, t_k)$ between two successive image frames (registered at t_k and t_{k+1}) was calculated. The error σ in photon number produced by the Poisson statistics of the incident photons and the noise σ_{CCD} of the CCD sensor detection (approximately four counts *per* pixel) was estimated by the Gaussian law of error propagation.

$$\sigma[D_{Ph}(x, y, t')] = \sqrt{\sigma[(S_{Ph}(x, y, t'_{k+1})]^2 + \sigma[(S_{Ph}(x, y, t'_k)]^2 + 2\sigma^2_{CCD}}$$

The data stacks $S_{Ph}(x, y, t)$ (in case of low background) and $D_{Ph}(x, y, t')$ (in case of high background) were then used for high precision localization of single molecules (lateral) by adapting modified Gaussian model functions. To reduce the computing efforts, ROIs of typically 8 × 8 pixels were used, containing the signal.

Then a two dimensional Gaussian with a background gradient was fitted to the thresholded signals.

$$f(x, y) = p_1 exp[-\frac{(x - p_2)^2 + (y - p_3)^2}{p_4^2}]$$
$$+ p_5 + p_6(x - p_2) + p_7(y - p_3)$$

An appropriate set of values p_1–p_7 was used as start parameters that were then optimized by the application of a Levenberg–Marquardt algorithm.

The final results were analyzed for parameter plausibility by additional filters. In this way molecules were localized in an observation volume with a thickness corresponding to an "optical section" of 600 nm. For further details see ref. [28].

3 Results

3.1 The label density is critical for 2CLM experiments

To test the effects of the localization accuracy and the density of fluorescent molecules on the appearance of the "nanoimages" obtained by 2CLM, the evaluation algorithms described above were applied to simulated data. As an example, results obtained from a simulated structure are presented. For this, the letters "2CLM" were scaled to an overall length of 2 µm and a height of 0.4 µm (first row in Fig. 2). These four letters were then simulated to contain single molecules with various densities (50 000, 5000, and 500/µm^2) displaying a "fluorescence burst" emission. From these original images, conventional epifluorescence images and 2CLM images were calculated as described in ref. [28].

In the second row of Fig. 2 the diffraction-limited widefield image shows some alterations in the intensity distribution and gives an estimate of the overall size of the "nanostructure." A reconstruction of the original object, however, is clearly not possible by assuming a "conventional" resolution (calculated PSF using numerical aperture of 1.4, 100 nm effective pixel size of the detector and 520 nm (560 nm red letters) as emission wavelength).

In the third row of Fig. 2 the image is shown for the application of the 2CLM approach assuming a mean localization accuracy of 20 nm; a comparison with the original "nanostructure" demonstrates the substantial resolution improvement. The forth row shows the simulation results for a localization accuracy of 10 nm. At a high (50 000/µm^2) or medium (5000/µm^2) molecule density, the original "2CLM nano-object" can be fully reconstructed. At a "low" molecule density, basic structural features can still be identified. To summarize, the simulations show (i) that the 2CLM method indeed allows us to extract structural information far below the conventional resolution limit of epifluorescence microscopy and (ii) that the density of molecules is a critical parameter, depending on the structure to be studied.

3.2 Nuclear distributions of H2A and Snf2H could be determined by 2CLM

The lateral distribution of mRFP1 labeled H2A and GFP labeled Snf2H proteins in human U2OS nuclei was determined by 2CLM within "optical sections" of about 600 nm thickness in about 20 cells. These

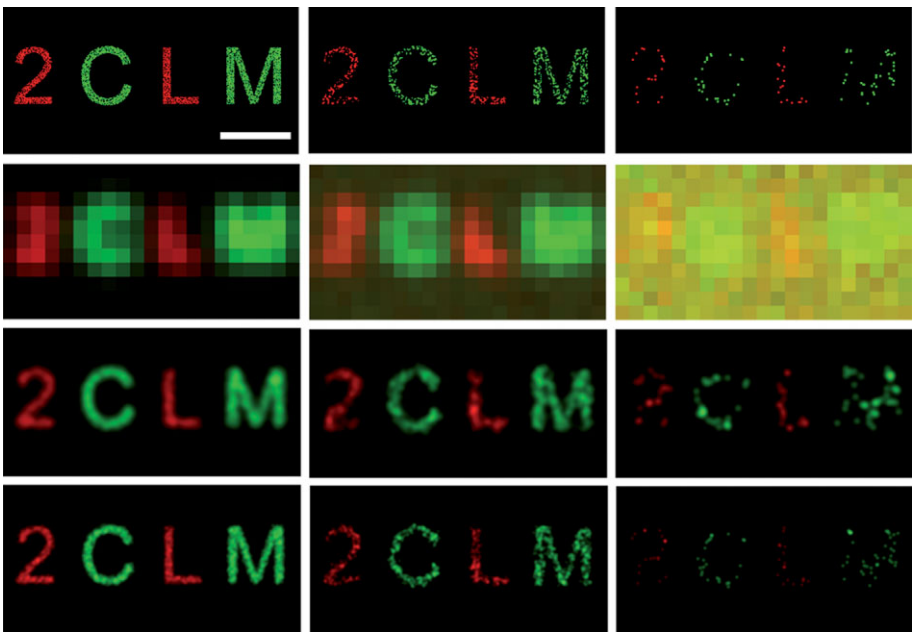

Figure 2. Simulation of 2CLM. First row: Dual color object in three different label densities (left: 50 000 molecules/µm^2, middle: 5000 molecules/µm^2, right: 500 molecules/µm^2). The size of the scale-bar ist 500 nm. Second row: Conventional epifluorescence microscopy with NA 1.4, 100 nm pixel size, 520/580 nm emission wavelength. Third row: 2CLM image with 20 nm mean localization accuracy. Last row: 2CLM image with 10 nm mean localization accuracy. The single molecule positions in the 2CLM images are blurred with a Gaussian kernel corresponding to the estimated mean localization accuracy of the process.

sections result from the fact, that the PSF of objects outside the focal plane is broadened up and thus has a worse S/N. Accordingly, these signals were filtered out by the fitting algorithm. On an average around 1200–1800 photons *per* molecule were detected.

Figure 3 shows the distribution of mRFP1 labeled H2A proteins in a human U2OS nucleus (size $12 \times 18\ \mu m^2$). A conventional epifluorescence image was experimentally recorded prior to the 2CLM measurement (Fig. 3A). The nucleoli can be clearly identified due to the lower content of H2A histone proteins. Due to the limited optical resolution no further details of the H2A distribution are apparent. The 2CLM data of the same nucleus are shown in Fig. 3B. A data stack consisting of 6000 individual images was recorded in four steps (1500 images acquired in each step due to the size of the PC memory) with a frame rate of about 16 Hz. Mechanical drift of the sample was corrected by correlating the summed signal of each of those four stacks with the first one. The drift within one data stack was estimated to be 12 nm (see Supporting Information).

In every image the positions of the blinking mRFP1 molecules were determined as described in Section 2.3. The result is displayed in Fig. 3B: All 71 156 registered positions of individual H2A-mRFP1 signals are plotted together and blurred with a Gaussian according to their localization accuracy. The mean localization accuracy was $\sigma = 38$ nm (see Fig. 6).

Figure 4 shows the distribution of GFP labeled Snf2H proteins in the same nucleus. Again a conventional epifluorescence image (Fig. 4A) was acquired before 2CLM imaging. Nucleoli cannot be identified in the epifluorescence nor the 2CLM image (Fig. 4). In total 4500 images were recorded in three stacks. From these, 47 062 positions of Snf2H were determined with a mean localization accuracy of $\sigma = 26$ nm (see also Fig. 6).

In Fig. 5 the signal of both fluorophores is shown in the appropriate colors for comparison. The same structures are visible in the epifluorescence (Fig. 5A) and the 2CLM image (Fig. 5B). Autofluorescence from unlabeled structures is not present in the 2CLM image.

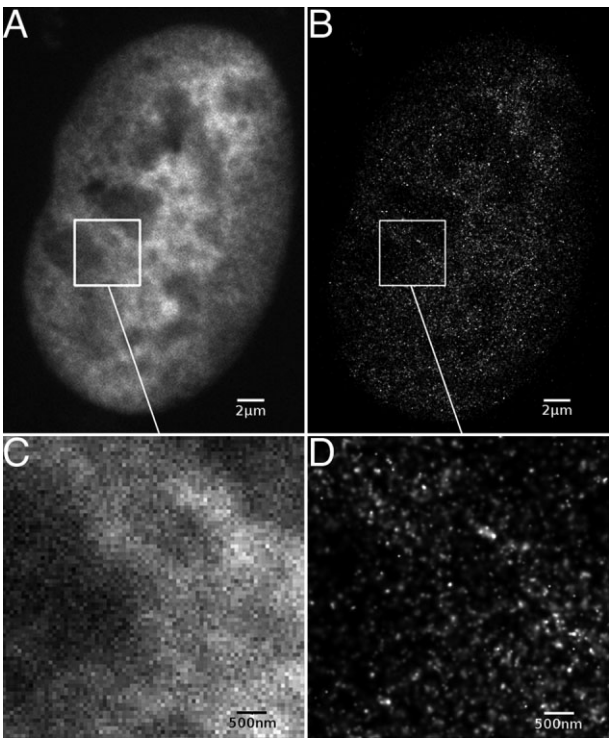

Figure 3. Distribution of H2A proteins within a human U2OS nucleus. (A) Conventional epifluorescence image. (B) 2CLM image, each mRFP1-position is blurred with a Gaussian representing the individual localization accuracy. Panel C and D display enlarged regions. Scale bars are 2 µm in A and B and 500 nm in C and D.

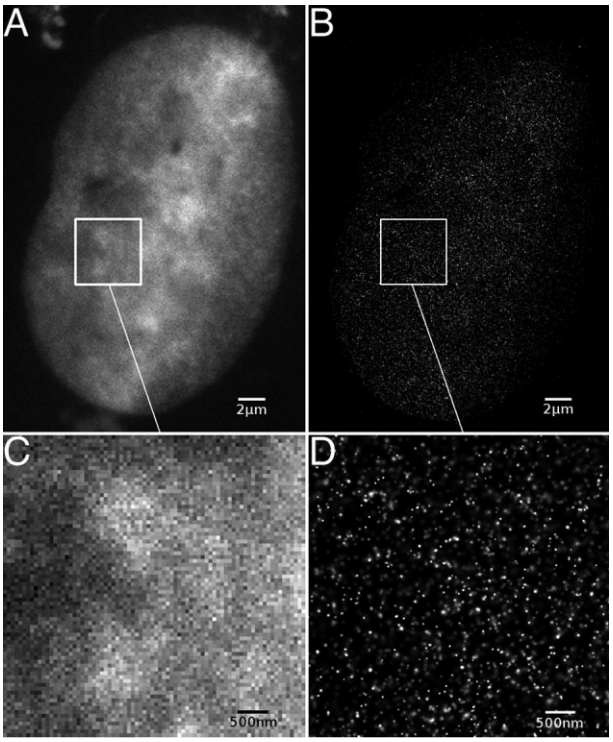

Figure 4. Distribution of Snf2H proteins within a human U2OS nucleus. (A) Conventional epifluorescence image. (B) 2CLM image, each GFP-position is blurred with a Gaussian representing the individual localization accuracy. Panel C and D display enlarged regions. Scale bars are 2 µm in A and B and 500 nm in C and D.

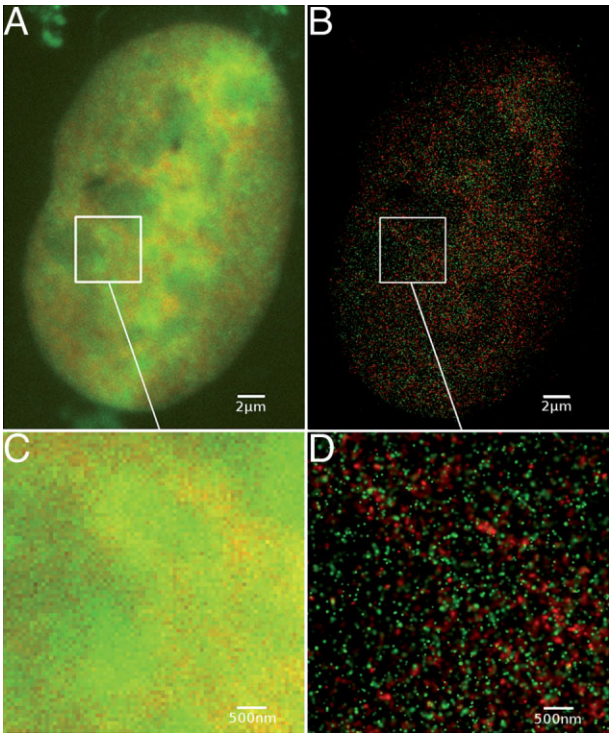

Figure 5. Distribution of H2A proteins (red) and Snf2H proteins (green) within a human U2OS nucleus. (A) Conventional epifluorescence image. (B) 2CLM image, each fluorochrome-position is blurred with a Gaussian representing the individual localization accuracy. Panel C and D display enlarged regions. Scale bars are 2 µm in A and B and 500 nm in C and D.

3.3 Distribution analysis revealed partial colocalization between H2A and Snf2H

To characterize the nuclear distributions of H2A and Snf2H, the number of neighbors of the same protein type within a 300 nm radius around each detected particle was determined in a typical cell and plotted into a histogram (Fig. 7A, B). As a reference, the same histogram was generated for random distributions with the corresponding particle densities. The histograms for the random distributions could be fitted with a single Gaussian, whereas the observed histograms for H2A and Snf2H were broader and had to be fitted with the sum of two or three Gaussians. This reflects the heterogeneity in the H2A and Snf2H density and the presence of low- and high-density populations for both H2A and Snf2H. To identify these regions of different particle density, different colors were assigned (Fig. 7C, D). The cut-off values were chosen to be the values at the intercept of the Gaussians used for fitting the corresponding histogram. In order to detect also locations with the highest protein density, the 10% of the particles with the largest number of neighbors were depicted in yellow. In the case of H2A, the sparse regions contained the nucleoli as expected. However, additional regions which did not coincide with these nuclear compartments appeared to be H2A-poor. The high-density regions of H2A (labeled green/yellow in Fig. 7C), which comprised about 55% of the area of the cell nucleus, formed interconnected patches including mostly regions located in the center of the nucleus. In the case of Snf2H, the sparse regions were found at the nuclear periphery. In the remaining part of the nucleus Snf2H was distributed more homogeneously than H2A. In contrast to the H2A distribution, the high-density regions of Snf2H (labeled green/yellow in Fig. 7D) comprised 36% of the area of the cell nucleus. In average, Snf2H molecules had 37 ± 12 neighbors, H2A molecules had 52 ± 23 neighbors (intervals include 68% of the molecules). Snf2H-rich regions were located near the center of the nucleus and often but not always, corresponded to H2A-rich regions (see arrows in Fig. 7 C/D).

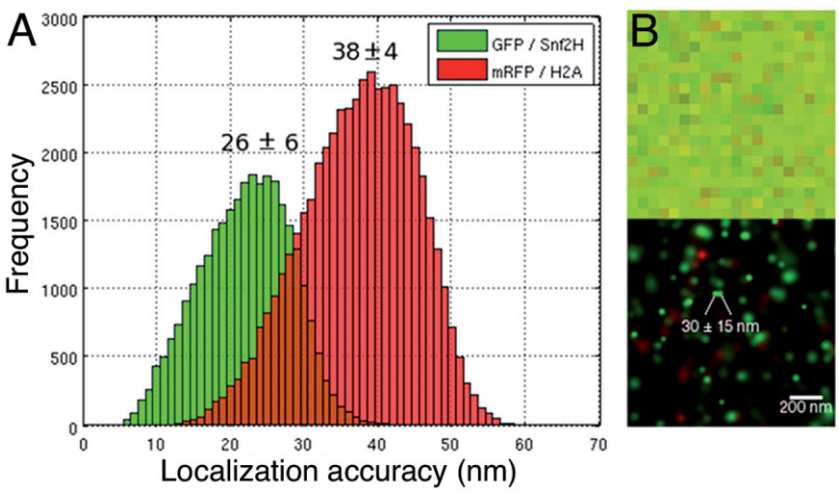

Figure 6. Localization accuracy. (A) Histogram of localization accuracies of GFP and mRFP1 determined by the fitting algorithm for one cell. The lower accuracy for mRFP1 (38 ± 4 nm) was due to a lower number of photon counts (see Supporting Information). (B) Comparison of conventional epifluorescence and 2CLM image. In the latter one, two molecule positions with a distance of about 30 nm can be resolved (both recorded within 7 s, corresponding to an estimated drift of about 1 nm). The pixel size in the epifluorescence image is 65 nm.

Biotechnol. J. 2009, 4, 927–938

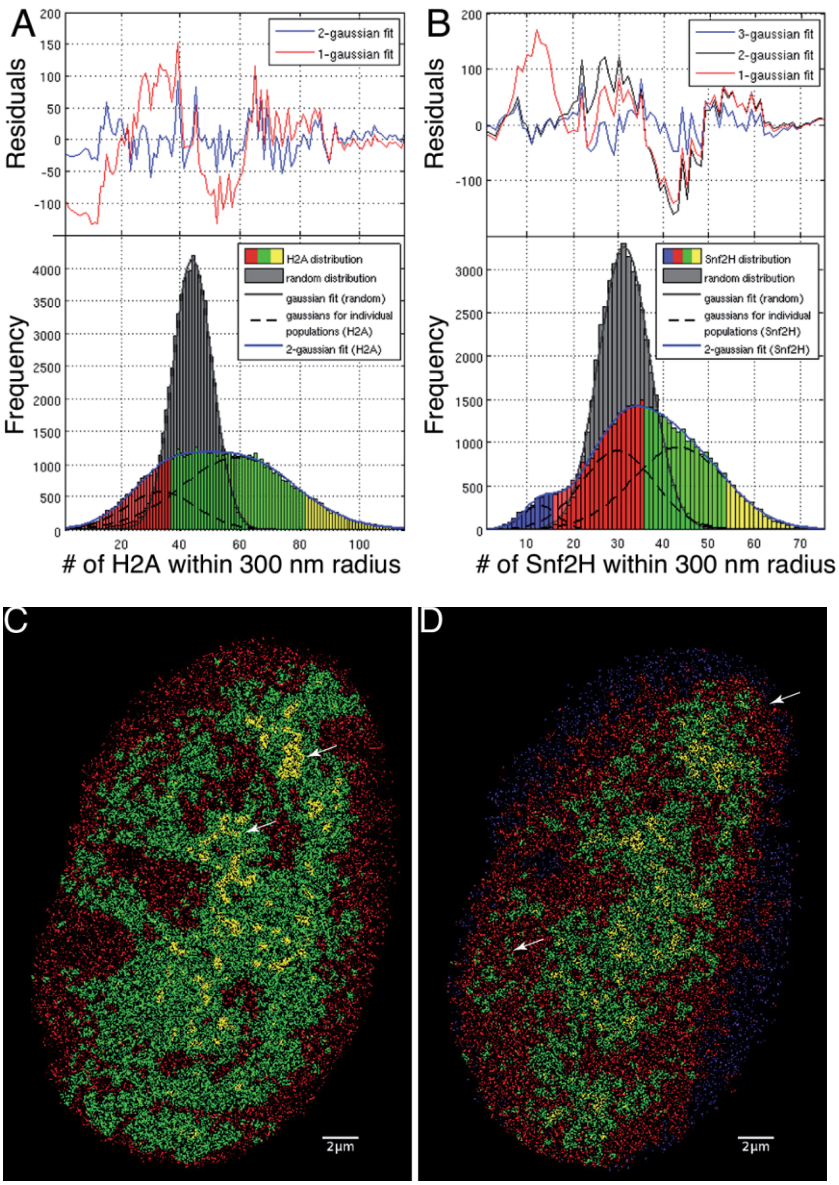

Figure 7. Visualization of particle densities. A histogram of the number of neighbors (of the same color) within a circle of 300 nm radius was plotted for H2A (A) and Snf2H (B) for the cell below. As a reference, the same histograms were plotted for random distributions with equal particle densities. Experimentally observed histograms were broader than the histograms for random distributions and could only be fitted considering different particle populations. Based on these histograms, density maps for H2A (C) and Snf2H (D) were derived to separate particles in the low-density population (blue/red), the high-density population (green), and the densest 10% (yellow). Arrows in panel C highlight regions of colocalization between H2A and Snf2H, arrows in panel D highlight regions of anti-colocalization.

To analyze the colocalization of H2A and Snf2H, a correlation coefficient according to Pearson of $R = 0.25$ was calculated for the images from Fig. 5, while R = 0.13–0.17 was obtained for the random distributions. A value of 1 would represent perfect colocalization, a value of –1 would represent perfect anti-colocalization. These results suggest a partial colocalization between H2A and Snf2H that is compatible with transient interaction behavior of the two proteins detected in FRAP experiments (data not shown). Similar results were obtained by the analysis of the number of Snf2H molecules around H2A in a typical cell and *vice versa* (Fig. 8). The average number of Snf2H molecules in the vicinity of H2A (50 molecules within 300 nm radius) was significantly larger than the average number of randomly distributed particles in the same region (41 molecules within 300 nm radius) as confirmed by a Kolmogorov-Smirnov test (see Supporting Information); the same was true for H2A molecules in the vicinity of Snf2H (33 H2A molecules *versus* 27 randomly distributed molecules within 300 nm radius). Further analysis of the histograms in Fig. 8 was indicative of the presence of two particle populations, one with a large number of neighbors and one with a small number of neighbors. Thus, the relative amounts of H2A and Snf2H differ throughout the cell, suggesting the presence of chromatin regions with locally enriched Snf2H concentration.

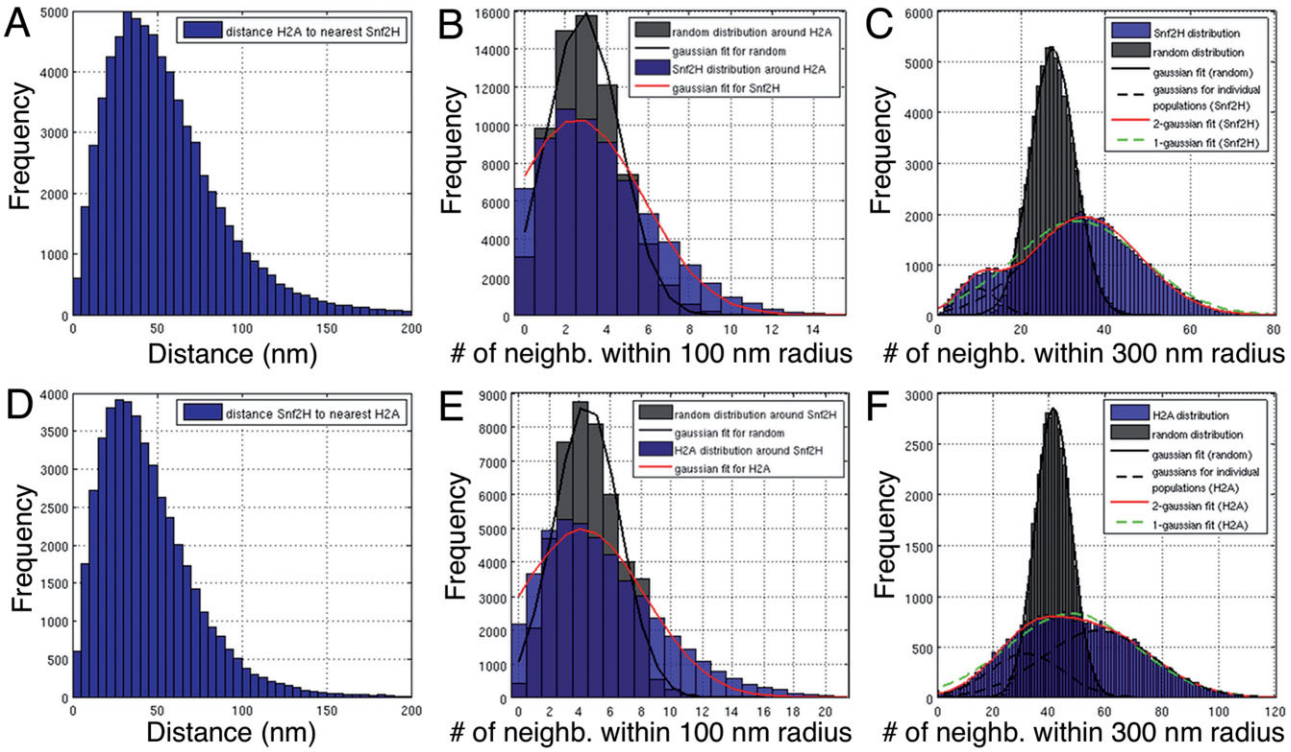

Figure 8. Colocalization analysis of H2A and Snf2H. For H2A (A) and Snf2H (D) in a typical cell a histogram of the distance to the nearest neighbor in the other color was plotted. Based on the average distances, two length-scales were chosen for which the number of differently colored neighbors was shown in a histogram (B, C, E, F). As a reference, the number of neighbors in a random distribution with corresponding densities is shown. Experimentally observed histograms were broader than the histograms for random distributions, reflecting the heterogeneity of the density. Furthermore, the average number of neighbors is larger than for a random distribution, suggesting partial colocalization between H2A and Snf2H.

4 Discussion

For the better understanding of functional cellular nanostructures, there is an urgent need to circumvent the limitations of conventional light microscopy given by the Abbe/Rayleigh limit of optical resolution. Multiple approaches for the light optical analysis of biostructures at enhanced resolution exist, with each of these having specific biological, biophysical, and biomedical applications. Recently, various methods of SALM have been shown to allow the nanoimaging of individual molecules at an optical resolution close to the dimensions of small proteins.

In this report, SPDM with conventional fluorochromes under special physical conditions was used to realize 2CLM. For each fluorochrome, only one Raser wavelength was sufficient. In this manner, the spatial distribution of two different molecule types with distinct fluorescence emission wavelengths was obtained.

Under the conditions used (sampling time *per* image being 60–100 ms) the percentage of molecules appearing multiple times was estimated to be rather low. In previous publications, using setups with the same mechanical stability and registration/evaluation conditions [28], single molecule positions of fluorescent proteins can be distinguished outside the nucleus, *i.e.* at very low molecule densities. A major percentage of multiple appearance would have resulted in multiple small clusters. This was not observed. Furthermore, in the 2CLM images presented here, a major percentage of multiple appearance should be reflected in a strongly increased frequency of next neighbor distances (Fig. 8) which also was not observed.

Since biological specimens labeled with fluorescent proteins are most common, 2CLM methods using such fluorochromes have a wide range of applications, including the potential for *in vivo* measurements in cell cultures. In particular, they offer unique possibilities for the characterization of molecular interactions between protein complexes. This is demonstrated in the present work for the determination of the spatial distribution of the Snf2H chromatin remodeler with respect to histone H2A as a nucleosome/chromatin marker. Although chromatin remodeling complexes have been

shown in several studies to possess distinct nucleosome/DNA binding and remodeling capabilities *in vitro* (*e.g.* [41–44] and references therein), little is known on how they operate in the cell. In a previous pioneering study Varga-Weisz and coworkers used conventional confocal fluorescence microscopy at a lateral resolution of several 100 nm to study Snf2H and its associated Acf1 subunit [45]. Their work revealed the overall Snf2H/Acf1 nuclear distribution with an enrichment in pericentric heterochromatin foci present in mouse cells, which have typical diameters of ~1 μm. 2CLM allowed an effective optical resolution that was better by an order of magnitude so that the light microscopic investigation of the interaction of Snf2H and other chromosomal proteins on the level of a single nucleosome becomes feasible. We show how density maps with high resolution for two different proteins in the same specimen can be generated and used to derive information about the interaction behavior on different length scales (Fig. 8). On these images, regions of increased nucleosome density can be identified from the H2A-mRFP1 signal, which could represent higher order structures of the folded nucleosome chain. The Snf2H remodeler is distributed more homogeneously suggesting that a significant fraction of Snf2H is not associated permanently with chromatin consistent with fluorescence recovery after photobleaching experiments (Erdel & Rippe, private communication). While the nuclear periphery was partially depleted from Snf2H, virtually all other nuclear regions, including the nucleolus, were accessible to the chromatin remodeler.

In Fig. 7 several distinct regions with locally increased or decreased Snf2H density with respect to H2A density are present that reflect a spatially altered interaction behavior between Snf2H and H2A. In particular, several high-density Snf2H regions can be identified that do not coincide with a strong H2A signal. Since it is expected that this increased Snf2H density is connected with higher remodeling activity, these regions represent *bona fide* chromatin remodeling hot spots that are likely to be loci of a pronounced translocation of nucleosomes by Snf2H-containing molecular machines. Furthermore, sites of colocalization of H2A and Snf2H are clearly present as inferred from the quantitative analysis (Fig. 8). The closely co-localizing signals of single Snf2H-GFP and H2A-mRFP1 proteins may be interpreted as complexes of Snf2H at a nucleosome. Thus, complexes of the chromatin remodeler with its substrate can be detected by 2CLM. Compared with fluorescence resonance energy transfer (FRET) methods, 2CLM images together with neighborhood estimates allow such vicinity determinations of single complexes at distances not accessible to FRET procedures. Additionally, 2CLM methods provide "true optical resolution" in the region of about ten times better than conventional fluorescence microscopy techniques and thus give also the spatial position of such complexes even in a "crowded" nucleus. We anticipate that further studies along these lines in combination with quantitative image analysis will provide valuable information on the molecular details of nucleosome translocations by chromatin remodelers. Furthermore, the 2CLM investigations of other chromosomal proteins associated with the genome will serve to derive spatial molecular interaction maps for their organization in the nucleus.

At an effective optical resolution down to the 10–20 nm range laterally in an optical section of about 600 nm thickness, numerous other applications in the structural elucidation of cellular nanostructures are feasible. Examples for such nanostructures are individual gene domains in genetically active and inactive states [2], environmentally induced changes of chromatin nanostructure [16], size and nuclear distribution of transcription complexes [48, 49], replication factories [50] and repair complexes [51], nuclear pore complex distribution [52], and arrangement of polyribosomes. An additional important application will be the possibility to count single molecules. Although the 2CLM technique allowed us to register only a part of all labeled molecules, the figures obtained are minimum absolute numbers. For example, a count of 90 000 proteins in an optical section of a human fibroblast nucleus of $10 \times 10\ \mu m^2 = 100\ \mu m^2$ results in a density of about 900 proteins per μm^2. Even at the best corresponding conventional optical resolution, only a few thousand molecules would be resolvable in a nuclear area of 100 μm^2, corresponding to a density of resolved molecules of about 30 molecules/μm^2. Since many protein types in the cells occur in numbers in the order of 10^4 to 10^5, 2CLM and related SALM methods for the first time promise to count fluorescently labeled molecules in the cell even at such high numbers and densities. Presently, the number of molecules counted is a relative number since it is not known to what percentage the molecules can be excited in the way required for this type of localization microscopy (which might be true also for other SALM methods). It is expected that by appropriate calibration methods, even absolute numbers of individual molecules will become countable, down to only a few molecules of a given type in an entire cell. If conditions can be realized to induce fluorescence in a substantial part of such molecules, the sensitivity of this method might become superior even to tech-

niques based on radioactive decay: To reliably determine the number of a few radioactively labeled molecules in a cell, one has to apply registration for at least several life times of the radioactive substance used for labeling. For radioactive elements used in biology and medicine, these times would be prohibitively long. In addition to an effective optical resolution in the macromolecular range, this will open perspectives for many additional applications on the single cell level, such as high precision monitoring of specific DNA sequence amplification, gene expression, fast counting of virus particles inside and outside cells at a spatial resolution equivalent to conventional electron microscopy, counting of proteins in intracellular normal and pathological aggregates, or counting of drug molecules present in specific nanoregions across the cell membrane.

The authors thank Professor Markus Sauer (Bielefeld University), Dr. Michael Wassenegger (AIPlanta, Neustadt/Weinstraße) and Dr. Victor Sourjik (ZMBH, University of Heidelberg) for support. We are grateful to Patrick Varga-Weisz (Babraham Institute, Cambridge) for providing plasmid vectors. The financial support of the State of Baden-Württemberg and of the Deutsche Forschungsgemeinschaft (SPP1128) to both Christoph Cremer and Karsten Rippe (also grant Ri 1283/8-1) and of the European Union (In Vivo Molecular Imaging Consortium, www.molimg.gr) is gratefully acknowledged. We also thank our colleagues Thibaud Jegou, Thomas Ruckelshausen, David Baddeley, Jürgen Reymann, Alexander Brunner, Alexa von Bassewitz, Heinz Eipel, and Margund Bach for great support. Paul Lemmer is a Ph.D. student fellow of the Hartmut Hoffmann-Berling International Graduate School of Molecular and Cellular Biology of the University of Heidelberg and a member of the Excellence Cluster Cellular Networks of the University of Heidelberg; Rainer Kaufmann is a Ph.D. student fellow in a Frontierproject of the Marsilius College University Heidelberg.

The authors have declared no conflict of interest.

References

[1] Cremer, T., *Von der Zellenlehre zur Chromosomentheorie*, Springer-Verlag, Berlin Heidelberg 1985 (http://humangenetik. bio.lmu.de/service/downloads/buch_tc/index.html).

[2] Cremer, T., Cremer, C., Chromosome territories, nuclear architecture and gene regulation in mammalian cells. *Nat. Rev. Genet.* 2001, *2*, 292–301.

[3] Abbe, E., Beiträge zur Theorie des Mikroskops und der mikroskopischen Wahrnehmung. Archiv f. *mikroskopische Anatomie* 1873, *9*, 411–468.

[4] Rayleigh, L., On the theory of optical images, with special reference to the microscope. *Philos. Mag.* 1896, *42*, 167–195.

[5] Hell, S. W., Lindek, S., Cremer, C., Stelzer, E. H. K., Measurement of the 4Pi-confocal point spread function proves 75 nm axial resolution. *Appl. Phys. Lett.* 1994, *64*, 1335.

[6] Hell, S. W., Toward fluorescence nanoscopy. *Nat. Biotechnol.* 2003, *2*, 1347–1355.

[7] Heintzmann, R., Cremer, C., Lateral modulated excitation microscopy: Improvement of resolution by using a diffraction grating. *Proc. SPIE* 1999, *356*, 185–196.

[8] Gustafsson, M., Shao, L., Carlton, P. M., Wang, C. J. R. *et al.*, Three-dimensional resolution doubling in wide-field fluorescence microscopy by structured illumination. *Biophys. J.* 2008, *94*, 4957–4970.

[9] Hell, S. W., Far-field optical nanoscopy. *Science* 2007, *316*, 1153–1158.

[10] Schmidt, R., Egner, A., Hell, S. W., isoSTED Microscopy. *Frontiers in Optics* (FiO) Rochester, NY, USA October 19, 2008, OSA Technical Digest (CD) (Optical Society of America, 2008), paper FTuS2 (http://www.opticsinfobase.org/abstract.cfm?URI=FiO-2008-FTuS2).

[11] Bornfleth, H., Sätzler, E. H. K., Eils, R., Cremer, C., High-precision distance measurements and volume-conserving segmentation of objects near and below the resolution limit in three-dimensional confocal fluorescence microscopy. *J. Microsc.* 1998, *189*, 118–136.

[12] Cremer, C., Hausmann, M., Bradl, J., Rinke, B., EP 1997953660, (1999); JP 1998528237, (1999); US 09331644, (1999**).**

[13] Heilemann, M., Herten, D. P., Heintzmann, R., Cremer, C. *et al.*, High-resolution colocalization of single dye molecules by fluorescence lifetime´ imaging microscopy. *Anal. Chem.* 2002, *74*, 3511–3517.

[14] Cremer, C., Edelmann, P., Bornfleth, H., Kreth, G. *et al.*, Principles of spectral precision distance confocal microscopy for the analysis of molecular nuclear structure, in: Jähne, B., Haußecker, H., Geißler, P. (Eds.), *Handbook of Computer Vision and Applications*, Academic Press, Inc. Orlando 1999, pp. 839–857.

[15] Edelmann, P., Esa, A., Hausmann M., Cremer, C., Confocal laser scanning microscopy: In situ determination of the confocal point-spread function and the chromatic shifts in intact cell nuclei. *Optik* 1999, *110*, 194–198.

[16] Esa, A, Edelmann, P., Kreth, G., Trakhtenbrot, L. *et al.*, Three-dimensional spectral precision distance microscopy of chromatin nanostructures after triple-colour DNA labelling: A study of the BCR region on chromosome 22 and the Philadelphia chromosome. *J. Microsc.* 2000, *199*, 96–105.

[17] Lacoste, T. D., Michalet, X., Pinaud, F., Chemla, D. S. *et al.*, Ultrahigh-resolution multicolor colocalization of single fluorescent probes *BIOS* 2000, *97*, 9461–9466.

[18] Schmidt, M., Nagorni, M., Hell, S. W., Subresolution axial distance measurements in far-field fluorescence microscopy with precision of 1 nanometer. *Rev. Sci. Instrum.* 2000, *71*, 2742.

[19] Rauch J., Hausmann M., Solovei, I., Horsthemke B. *et al.*, Measurement of local chromatin compaction by spectral precision distance microscopy. *Proc. SPIE* 2000, *4164*, 1–9.

[20] Betzig, E., Patterson, G. H., Sougrat, R., Lindwasser, O. W. *et al.*, Imaging intracellular fluorescent proteins at nanometer resolution. *Science* 2006, *313*, 1642–1645.

[21] Hess, S., Girirajan, T., Mason, M. Ultra-high resolution imaging by fluorescence photoactivation localization microscopy. *Biophys. J.* 2006, *91*, 4258–4272.
[22] Rust, M., Bates, M., Zhuang, X., Sub-diffraction-limit imaging by stochastic optical reconstruction microscopy (STORM). *Nat. Methods* 2006, *3*, 793–795.
[23] Egner, A., Geisler, C., von Middendorff, C., Bock, H. *et al*., Fluorescence nanoscopy in whole cells by by asynchronous localization of photoswitching emitters. *Biophys. J.* 2007, *93*, 3285–3290.
[24] Andresen, M., Stiel, A. C., Jonas, F., Wenzel, D. *et al*., Photoswitchable fluorescent proteins enable monochromatic multilabel imaging and dual color fluorescence nanoscopy. *Nat. Biotechnol.* 2008, *26*, 1035–1040.
[25] Reymann, J., Baddeley, D., Gunkel, M., Lemmer, P. *et al*., High-precision structural analysis of subnuclear complexes in fixed and live cells via spatially modulated illumination (SMI) microscopy. *Chromosome Res.* 2008, *16*, 367–382.
[26] Lemmer, P., Gunkel, M., Baddeley, D., Kaufmann, R. *et al*., SPDM: Light microscopy with single-molecule resolution at the nanoscale. *Appl. Phys. B* 2008, *93*, 1–12.
[27] Heilemann M., van de Linde S., Schuttpelz M., Kasper R. *et al*., Subdiffraction-resolution fluorescence imaging with conventional fluorescent probes. *Angew. Chemie, Int. Ed. 47*, 6172–6176.
[28] Kaufmann, R., Lemmer, P., Gunkel, M., Weiland Y. *et al*., SPDM – Single molecule superresolution of cellular nanostructures. *Proc. SPIE* 2009, *7185*, 71850J.
[29] Fölling, J., Bossi, M., Bock, H., Medda, R. *et al*., Fluorescence nanoscopy by ground-state depletion and single-molecule return. *Nat. Methods* 2008, *5*, 943–945.
[30] S. van de Linde, M Sauer, M Heilemann, Subdiffraction-resolution fluorescence imaging of proteins in the mitochondrial inner membrane with photoswitchable fluorophores. *J. Struct. Biol.* 2008, *164*, 250–254.
[31] van de Linde, S., Kasper, R., Heilemann, M., Sauer, M., Photoswitching microscopy with standard fluorophores. *Appl. Phys. B* 2008, *93*, 725–731.
[32] Rittweger, E., Han, K. Y., Irvine, S. E., Eggeling, C. *et al*., STED microscopy reveals crystal colour centres with nanometric resolution. *Nat. Photonics* 2009, *3*, 144–147.
[33] Burns, D. H., Callis, J. B., Christian, G. D., Davidson, E. R., Strategies for attaining superresolution using spectroscopic data as constraints. *Appl. Opt.* 1985, *24*, 154–161.
[34] Betzig, E., Proposed method for molecular optical imaging. *Opt. Lett.* 1995, *20*, 237.
[35] van Oijen, A. M., Köhler, J., Schmidt, J., Müller, M. *et al*., 3-Dimensional super-resolution by spectrally selective imaging. *Chem. Phys. Lett.* 1998, *192*, 182–187.
[36] Sinnecker, D., Voigt, P., Hellwig, N., Schaefer, M., Reversible photobleaching of enhanced green fluorescent proteins. *Biochemistry* 2005, *44*, 7085–7094.
[37] Patterson, G. H., Lippincott-Schwartz, J., A photoactivatable GFP for selective photolabeling of proteins and cells. *Science* 2002, *297*, 1873–1877.
[38] Hendrix, J., Flors, C., Dedecker, P., Hofkens, J. *et al*., Dark states in monomeric red fluorescent proteins studied by fluorescence correlation and single molecule spectroscopy. *Biophys. J.* 2008, *94*, 4103.
[39] Baddeley D., Jayasinghe I. D., Cremer C., Cannell M. B. *et al*., Light-induced dark states of organic fluorochromes enable 30 nm resolution imaging in standard media. *Biophys. J.* 2009, *2*, L22-L24.
[40] van Holde, K. E., *Chromatin*, Springer, Heidelberg 1989.
[41] Becker, P. B., Horz, W., ATP-dependent nucleosome remodeling. *Annu. Rev. Biochem.* 2002, *71*, 247–273.
[42] Cairns, B. R., Chromatin remodeling: Insights and intrigue from single-molecule studies. *Nat. Struct. Mol. Biol.* 2007, *14*, 989–996.
[43] Rippe, K., Schrader, A., Riede, P., Strohner, R. *et al*., DNA sequence- and conformation-directed positioning of nucleosomes by chromatin-remodeling complexes. *Proc. Natl. Acad. Sci. USA* 2007, *104*, 15635–15640.
[44] Langst, G., Becker, P. B., Nucleosome mobilization and positioning by ISWI-containing chromatin- remodeling factors. *J. Cell Sci.* 2001, *114*, 2561–2568.
[45] Collins, N., Poot, R. A., Kukimoto, I., Garcia-Jimenez, C. *et al*., An ACF1-ISWI chromatin-remodeling complex is required for DNA replication through heterochromatin. *Nat. Genet.* 2002, *32*, 627–632.
[46] Jegou, T., PhD Thesis, University Heidelberg 2007.
[47] Lemmer P., Gunkel M., Baddeley D., Kaufman R. *et al*., Using conventional fluorescent markers for far-field fluorescence nanoscopy allows resolution in the 10 nm range *J. Microsc*. in press.
[48] Rauch J., Knoch T. A., Solovei I., Teller K. *et al*., Lightoptical precision measurements of the active and inactive Prader-Willi Syndrome imprinted regions in human cell nuclei. *Differentiation* 2008, *76*, 66–83.
[49] Martin S., Failla A. V., Spoeri U., Cremer C. *et al*., Measuring the size of biological nanostructures with spatially modulated illumination microscopy. *Mol. Biol. Cell* 2004, *15*, 2449–2455.
[50] Leonhardt, H., Rahn, H. P., Weinzierl, P., Sporbert, A. *et al*., Dynamics of DNA replication factories in living cells. *J. Cell Biol.* 2000, *149*, 271–280.
[51] Hauptner, A., Krucken, R., Greubel, C., Hable, V. *et al*., DNA-repair protein distribution along the tracks of energetic ions. *Radiat. Prot. Dosimetry* 2006, *122*, 147–149.
[52] Schermelleh, L., Carlton, P. M., Haase, S., Shao, L. *et al*., Subdiffraction multicolor imaging of the nuclear periphery with 3d structured illumination microscopy, *Science* 2006, *320*, 1332–1336.

Biotechnology Journal

Supporting Information for DOI 10.1002/biot.200900005

Dual color localization microscopy of cellular nanostructures

Manuel Gunkel, Fabian Erdel, Karsten Rippe, Paul Lemmer, Rainer Kaufmann, Christoph Hörmann, Roman Amberger and Christoph Cremer

S1 Chromatic shift between $\lambda_{em} \approx 520$ nm and $\lambda_{em} \approx 585$ nm

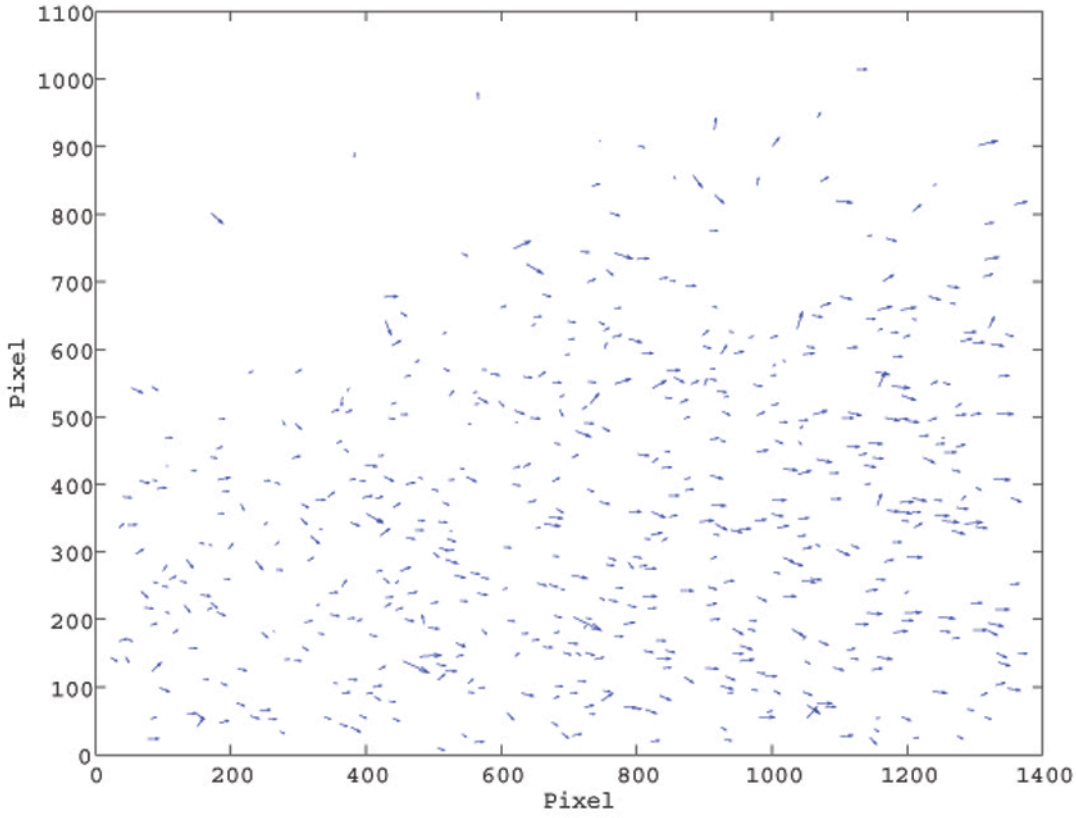

Figure S1: 100 nm beads fixed on object slides were excitated at $\lambda_{ex} = 488$ nm and λ_{ex} 568 nm, imaged and localized. The difference in localization is visualized as arrows, which point from the bead position obtained at $\lambda_{ex} = 488$ nm excitation (emission maximum at $\lambda_{em} = 520$ nm) to position obtained at $\lambda_{ex} = 568$ nm excitation (emission maximum at about $\lambda_{em} = 585$ nm), stretched by a factor of 150 in order to be visible at all. The mean chromatic shift was found to be 5.6 ± 2.3 nm. 1 pixel corresponds to 65 nm in the object plane.

S2 Relation between standard deviation σ and full width at half maximum FWHM

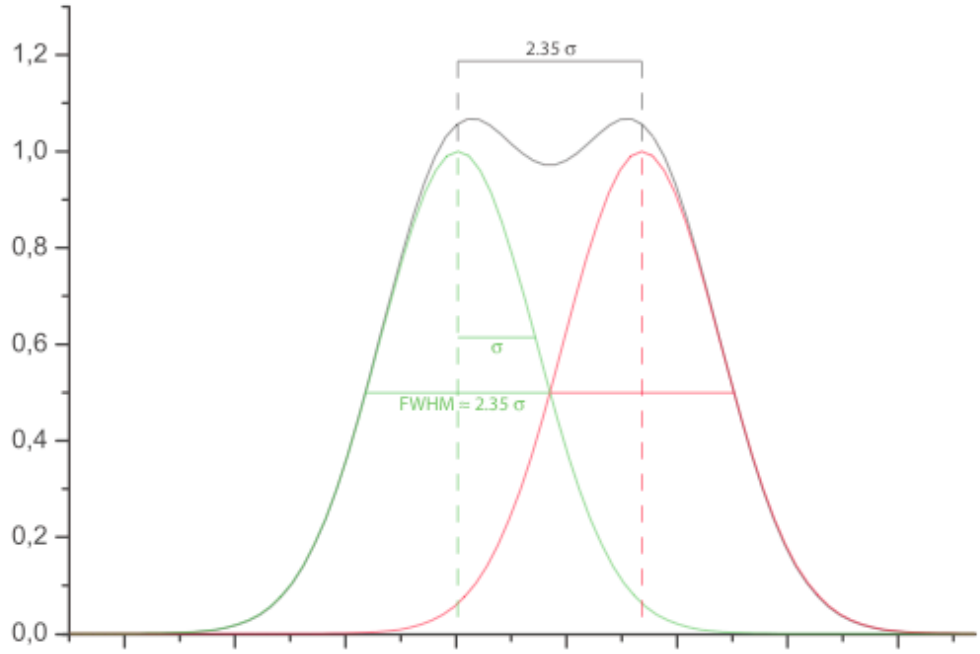

Figure S2: Relation between standard deviation σ and full width at half maximum FWHM. FWHM = 2.35σ. Two objects are optically resolved if the distance between them is larger than the FWHM.

S3 Gaussian with additional background gradient

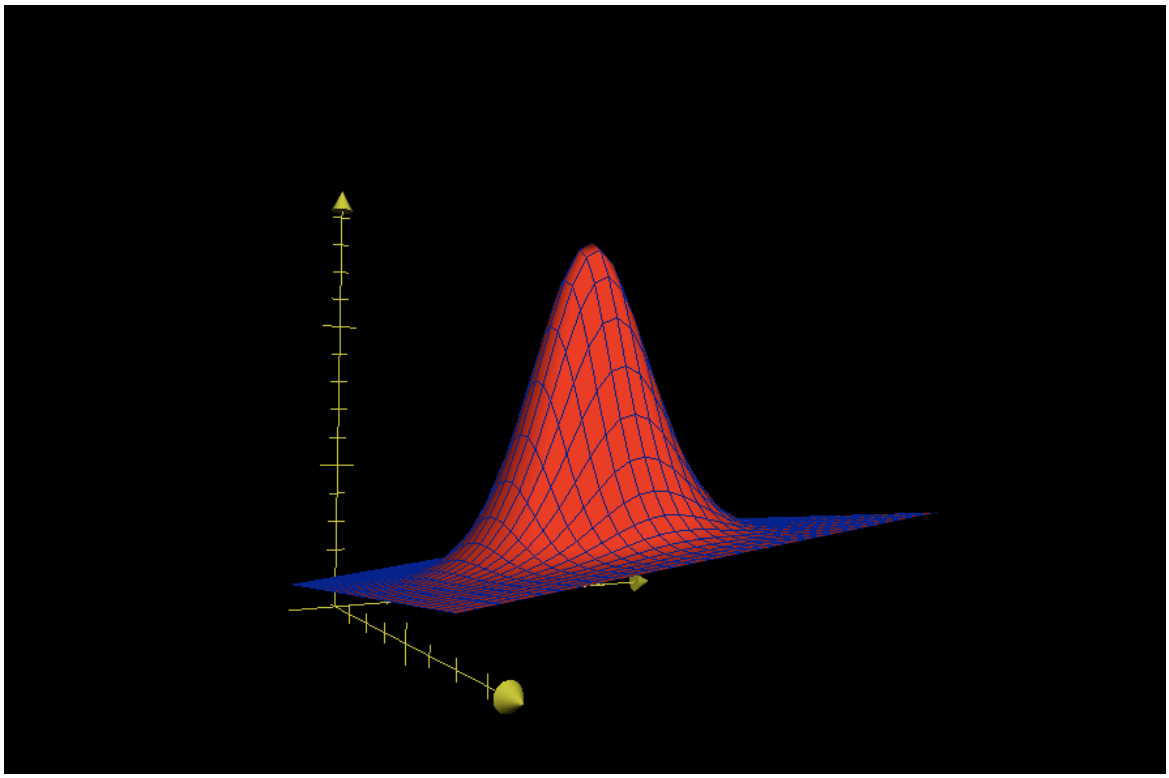

Figure S3: Two-dimensional Gaussian with an additional background gradient, as described by

$$f(x,y) = p_1 \exp(-\frac{(x-p_2)^2+(y-p_3)^2}{2{p_4}^2}) + p_5 + p_6(x-p_2) + p_7(y-p_3);$$

where $p_5 + p_6(x - p_2) + p_7(y - p_3)$ represents the background plane.

S4 Convergence of the fit algorithm

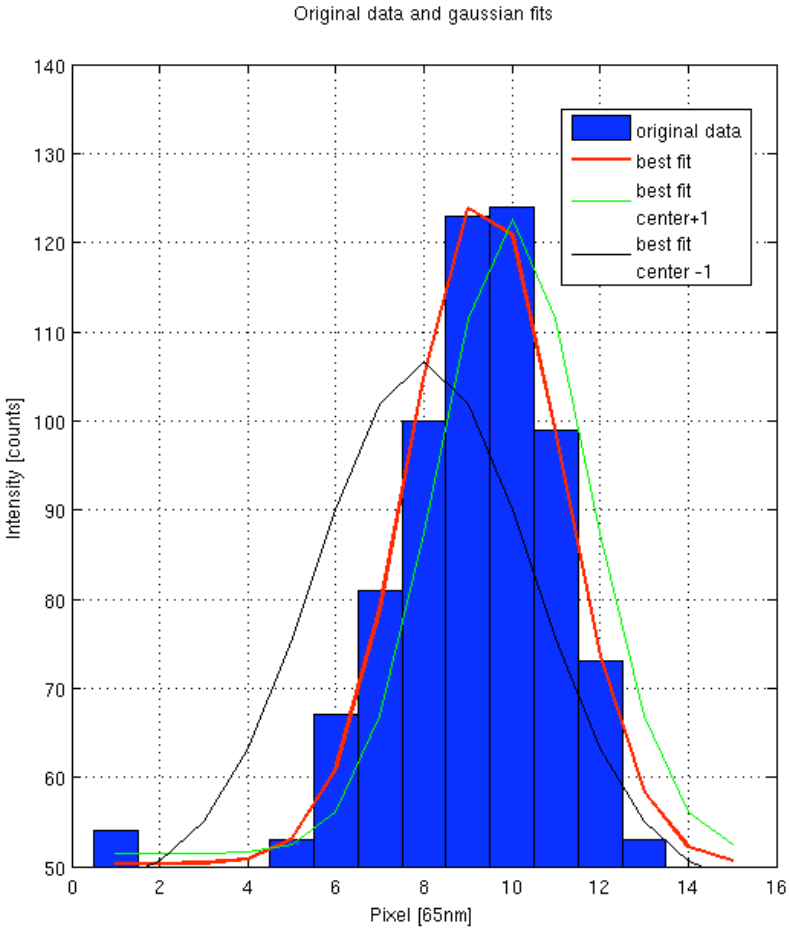

Figure S4a: Various gaussian fits to the original data at different maximum positions. The best result is obtained for the position found by the fit algorithm.

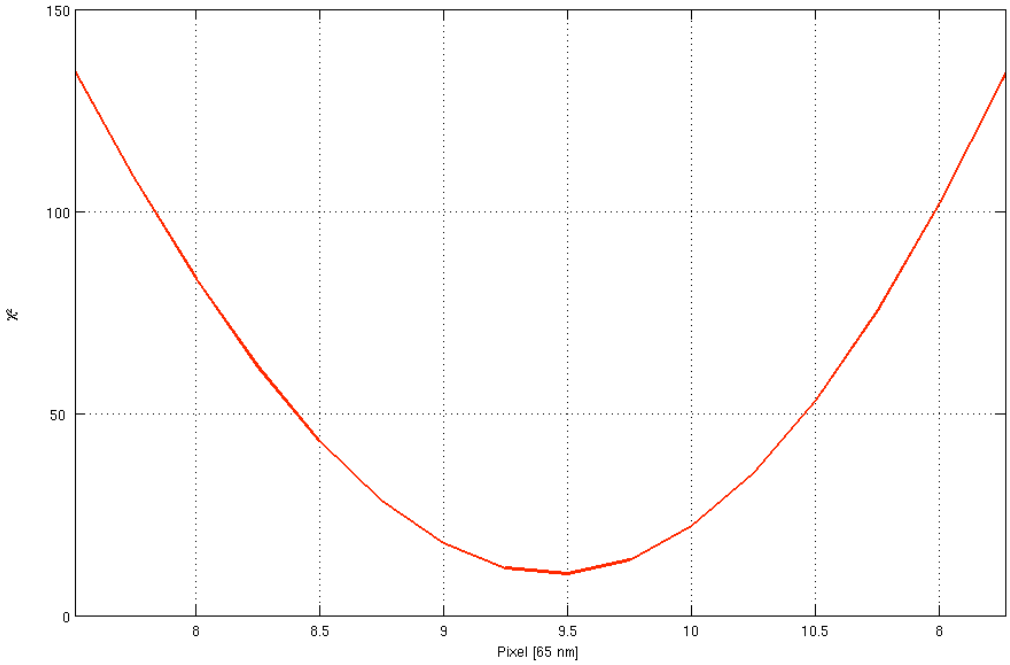

Figure S4b: χ^2 for a variation of the lateral position parameter of the Gaussian. The fit converges at the minimum.

S5 Kolmogorov-Smirnov test

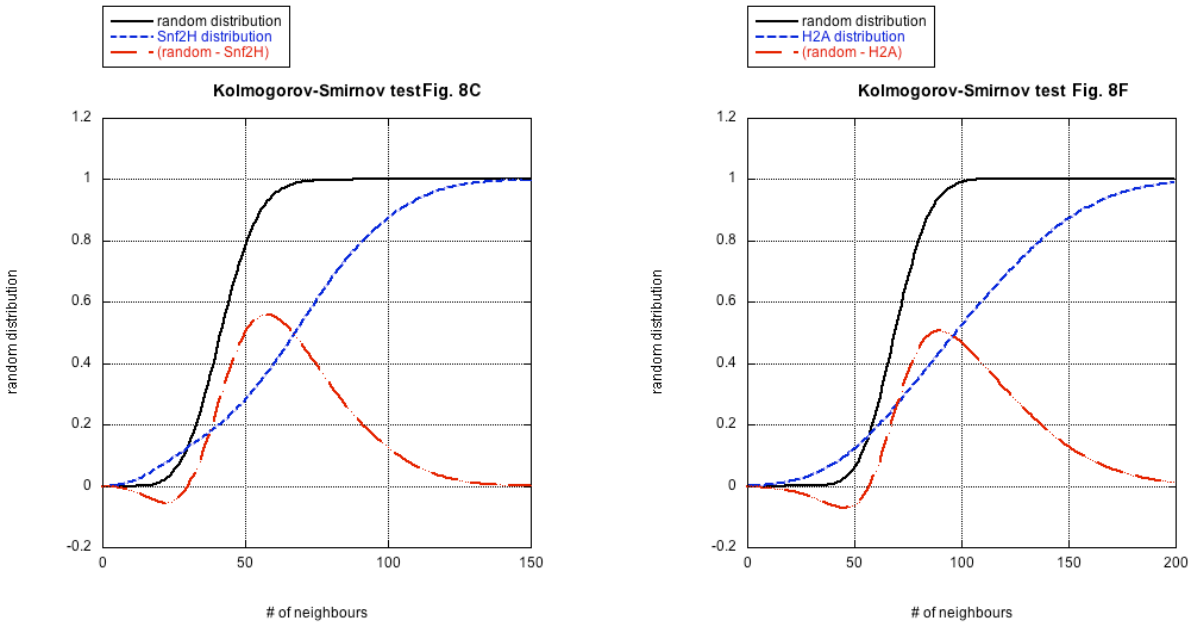

Figure S5: Kolmogorov-Smirnov test of Fig. 8C & 8F. The difference between the random point distributions and the experimental distributions is significant ($p < 0.05$). Calculation for 95 % confidence:

$$\sqrt{\left(\frac{n1 * n2}{(n1 + n2)}\right)} * sup_x * |F_1(x) - F_2(x)| = 117 > K_5 = 4 * 10^{-3}$$

S6 Mechanical drift

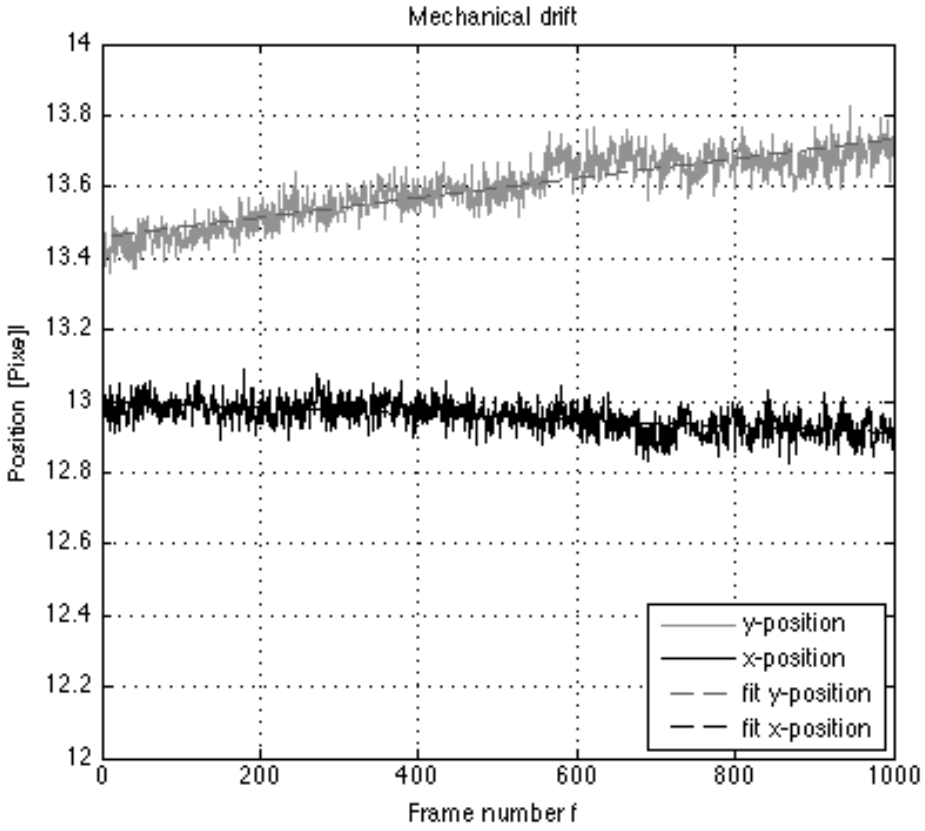

Figure S6: Drift of stage. The location of 1 identified bead was determined every 50 ms. Ordinate: x/y position, abscissa: frame number (f = 1000 corresponds to 1000 images registered in 50 s). Δx = -0.11 nm/s, Δy = 0.36 nm/s, $\Delta d_{total} = [\Delta x^2 + \Delta y^2]^{1/2}$ = 0.37 nm/s. 1Pixel corresponds to 65 nm.